Out-of-time-order correlator for the van der Waals potential

Hui Li[®], Eli Halperin, Reuben R. W. Wang[®], and John L. Bohn[®] *JILA*, *NIST and Department of Physics, University of Colorado, Boulder, Colorado 80309, USA*

(Received 19 January 2023; accepted 8 March 2023; published 22 March 2023)

The quantum-to-classical correspondence is often quantified in dynamics by the out-of-time-order correlator (OTOC). In chaotic systems, the OTOC is expected to grow exponentially at early time, characteristic of a Lyapunov exponent; however, exponential growth can also occur for integrable systems. Here we investigate the OTOC for realistic diatomic molecular potentials in one degree of freedom, finding that the OTOC can grow exponentially near the dissociation energy of the molecule. Further, this dynamics is tied to the classical dynamics of the atoms at the outer classical turning point of the potential. These results should serve to guide and interpret dynamical chaos in more complex molecules.

DOI: 10.1103/PhysRevA.107.032818

I. INTRODUCTION

The link between quantum-mechanical and classical physics remains an elusive one. Currently, one of the frontline efforts in forging this link seeks quantum-mechanical quantities whose time evolution depends sensitively on an initial condition, reminiscent of the Lyapunov exponent in classical chaos [1–15]. One such quantity, and the one we consider here, is the out-of-time-order correlator (OTOC) [4,16,17]. We will introduce and define this quantity in our context below, but here we note that it is at least a partial success: For example, in a model problem such as a pair of nonlinearly coupled harmonic oscillators, the quantum-mechanical OTOC grows exponentially in time under the same circumstances in which the classical system exhibits positive Lyapunov exponents [18].

Not all mechanical systems are chaotic, however. In particular, nondissipative motion in a single degree of freedom, with a time-independent Hamiltonian, is always integrable (having at least total energy as a constant of the motion). The OTOC has been studied in various such instances, finding that it does indeed show exponential growth in certain situations, such as an inverted harmonic-oscillator potential, where classical trajectories also depend exponentially sensitively on initial conditions [7,19–21]. If not chaotic, let us at least refer to this kind of behavior as sensitive. Conversely, in restoring potentials such as a regular harmonic oscillator [17] or a power-law potential proportional to x^{2N} [22], exponential growth is seen in neither the classical dynamics nor in the OTOC, a situation that might be termed regular. Thus it appears that the OTOC may serve as a quantum-to-classical link in dynamics, irrespective of the chaotic nature of that dynamics.

In this paper we extend the work on OTOCs in onedimensional systems to potentials that exist between atoms in a molecule, for example, a schematic Lennard-Jones potential, as well as the realistic singlet potential between ground-state rubidium atoms. Such potentials present a unique opportunity to explore the behavior of the OTOC for the following reasons.

- (i) The low-lying energy eigenstates are well represented by harmonic oscillators and hence show no exponential sensitivity to either classical initial conditions or the OTOC.
- (ii) By contrast, higher-lying very anharmonic states can show an exponential dependence on both these quantities. Thus a transition from regular to sensitive behavior can be described.
- (iii) Wave functions of the high-lying states are strongly concentrated at the outer classical turning point r_c of the potential. As we will see, this emphasizes the essentially local character of the quantum-to-classical link, at least at short times, and its ultimate origin in the sign of the curvature of the potential near r_c .

Ruminations of this sort are of interest beyond a single degree of freedom. For example, it has been established experimentally that weakly bound dimers of lanthanide atoms, explored in ultracold gases, show hints of quantum chaos via a standard signature, namely, their nearest-neighbor level spacings exhibit statistics close to those implied by the Gaussian orthogonal ensemble in random matrix theory [23,24]. This kind of chaos is expected to be driven by strong nonlinear couplings between the rovibrational and spin degrees of freedom of these highly multichannel molecules [25,26]. Demonstrable chaos in the molecules' dynamics is however yet to be addressed, either theoretically or experimentally. It is conceivable that the OTOC would be the means to do so, but for this approach to be viable, we must first understand how the OTOC works in a single molecular channel so that mere sensitivity will not be mistaken for truly chaotic behavior. It is also worth noting that exponentially growing OTOCs also correlate to classical Lyapunov exponents in the spectra of polyatomic molecules [15].

The remainder of this work is structured as follows. After a brief definition in Sec. II, we describe the model systems used and the numerical methods to calculate the OTOC in Sec. III. Numerical results are presented in Sec. IV, and in Sec. V we detail an approximation to deduce the dependence of the exponential growth behavior. Finally, we draw our conclusions

with a discussion on the further possible research directions in Sec. VI.

II. DEFINITION

We begin in this section by explaining the definition of the OTOC in one dimension, using the generic coordinate x to represent this dimension. The quantum-mechanical OTOC is defined by a close analogy with classical dynamics. In one degree of freedom this is formulated as follows. For a generic classical Hamiltonian

$$H = \frac{p^2}{2m} + V(x),\tag{1}$$

Hamilton-Jacobi theory posits the ability to transform between alternative representations of coordinate and momentum [27]. In particular, a set of phase-space coordinates may be described by the initial position and momentum (x_0, p_0) and related to the time-evolving coordinates (x(t), p(t)) by an appropriate time-dependent canonical transformation [28]. The time-evolving coordinates are then explicit functions of the initial conditions, which in our immediate case can be written

$$x(t) = x_0 f(t) + \frac{p_0}{m\chi} g(t).$$
 (2)

Here f(t) and g(t) are solutions to the equations of motion, with initial conditions f(0) = 1, $\dot{f}(0) = 0$, g(0) = 0, $\dot{g}(0) = \chi$, and χ is a constant carrying units of frequency.

Written this way, the relation between x, at some time t, and its initial value x_0 is fairly explicit. This relation is revealed by computing the Poisson bracket

$$\{x(t), p_0\}_{x_0, p_0} = \frac{\partial x(t)}{\partial x_0} \frac{\partial p_0}{\partial p_0} - \frac{\partial x(t)}{\partial p_0} \frac{\partial p_0}{\partial x_0}$$
$$= \frac{\partial x(t)}{\partial x_0}, \tag{3}$$

which therefore denotes the dependence of x(t) on the initial condition x_0 . Thus, for a harmonic oscillator with $V(x) = m\omega^2 x^2/2$ and $\partial x(t)/\partial x_0 = \cos \omega t$, the dependence is regular rather than sensitive, whereas for an antioscillator, $V(x) = -m\lambda^2 x^2/2$ and $\partial x(t)/\partial x_0 = \cosh \lambda t$ soon evolving to approximately $e^{\lambda t}$, showing that the dependence is exponentially sensitive, where λ is analogous to the frequency scale ω in the harmonic oscillator. Note that classical sensitivity in these two cases is tied to the sign of the potential's curvature.

Thus defined, the quantity of interest is transported to the quantum realm in the conventional way, by replacing the Poisson bracket by a commutator, i.e., quantization, and by presenting operators in the Heisenberg representation. That is to say, given the quantum-mechanical Hamiltonian

$$\hat{H} = \frac{\hat{p}^2}{2m} + \hat{V}(\hat{x}) \tag{4}$$

and the Heisenberg-representation coordinate operator

$$\hat{x}(t) = e^{i\hat{H}t/\hbar}\hat{x}(0)e^{-i\hat{H}t/\hbar},\tag{5}$$

sensitivity to the initial condition would be expressed by the quantity

$$[\hat{x}(t), \hat{p}(0)]/i\hbar, \tag{6}$$

which is the quantum analog of Eq. (3). Two addenda are made to this procedure. First, one squares the commutator, lest its interesting parts average out, and second, one takes its average over a quantum state of interest; for us, this will be an energy eigenstate $|n\rangle$.

Thus, the OTOC for state n is defined as

$$C_n(t) = -\langle n|[\hat{x}(t), \hat{p}(0)]^2|n\rangle/\hbar^2. \tag{7}$$

This is a four-point correlation function evaluated between operators with the times appearing out of order, hence the name out-of-time-order correlator. The quantity $C_n(t)$ therefore defines a time-dependent number, allowing us to ascertain, for each n, whether $C_n(t)$ grows exponentially in time. More generally, one sometimes computes a thermal average of the $C_n(t)$'s, but we do not do so here. Using the classical-quantum correspondence $[\ ,\]/i\hbar \rightarrow \{\ ,\ \}$ and then

$$\frac{-\langle n|[\hat{x}(t), \hat{p}(0)]^2|n\rangle}{\hbar^2} \to \{x(t), p_0\}^2 = \left(\frac{\partial x(t)}{\partial x_0}\right)^2. \tag{8}$$

Thus, $C_n(t) = \cos^2(\omega t)$ for a harmonic oscillator [17], whereas for an antioscillator $C_n(t) = \cosh^2(\lambda t) \sim e^{2\lambda t}$ [21], indicating that the quantum sensitivity to the initial condition is twice that in the classical case.

III. MODEL AND COMPUTING METHODS

For the remainder of this article, we specialize to the case of vibrational motion of a diatomic molecule. To this end, we replace the generic coordinate x of the preceding section with the distance r between atoms. Further, we will denote the momentum conjugate to r by simply p, hopefully without causing confusion. We will use atomic units throughout.

We consider two similar situations. The first consists of identical structureless atoms, interacting via the Lennard-Jones potential

$$V(r) = \frac{C_{12}}{r^{12}} - \frac{C_6}{r^6},\tag{9}$$

where r is the interatomic separation. The second situation consists of two ground-state rubidium atoms, interacting via their $X^1\Sigma_g^+$ ground-state potential [29]. We keep the two situations similar, if not identical, by setting $C_6 = 4710E_ha_0^6$ in the Lennard-Jones potential equal to the C_6 coefficient for rubidium and by choosing $C_{12} = 3.05 \times 10^8 E_h a_0^{12}$ so that the two potentials have the same depth of $0.018E_h$, where E_h is the Hartree energy and a_0 is the Bohr radius. In both cases, we use the reduced mass $\mu = 43.45459$ amu of two rubidium atoms, where amu denotes the unified atomic mass unit. To constrain the motion in a single degree of freedom, we discard the molecular rotation in our model, i.e., the atoms interact in an s-wave channel.

The bound energy eigenstates of either potential are $|n\rangle$, with energy E_n . In terms of these, the OTOC as defined in Eq. (7) can be rewritten as

$$C_n(t) = \sum_{l} b_{nl}(t)b_{nl}^*(t),$$
 (10)

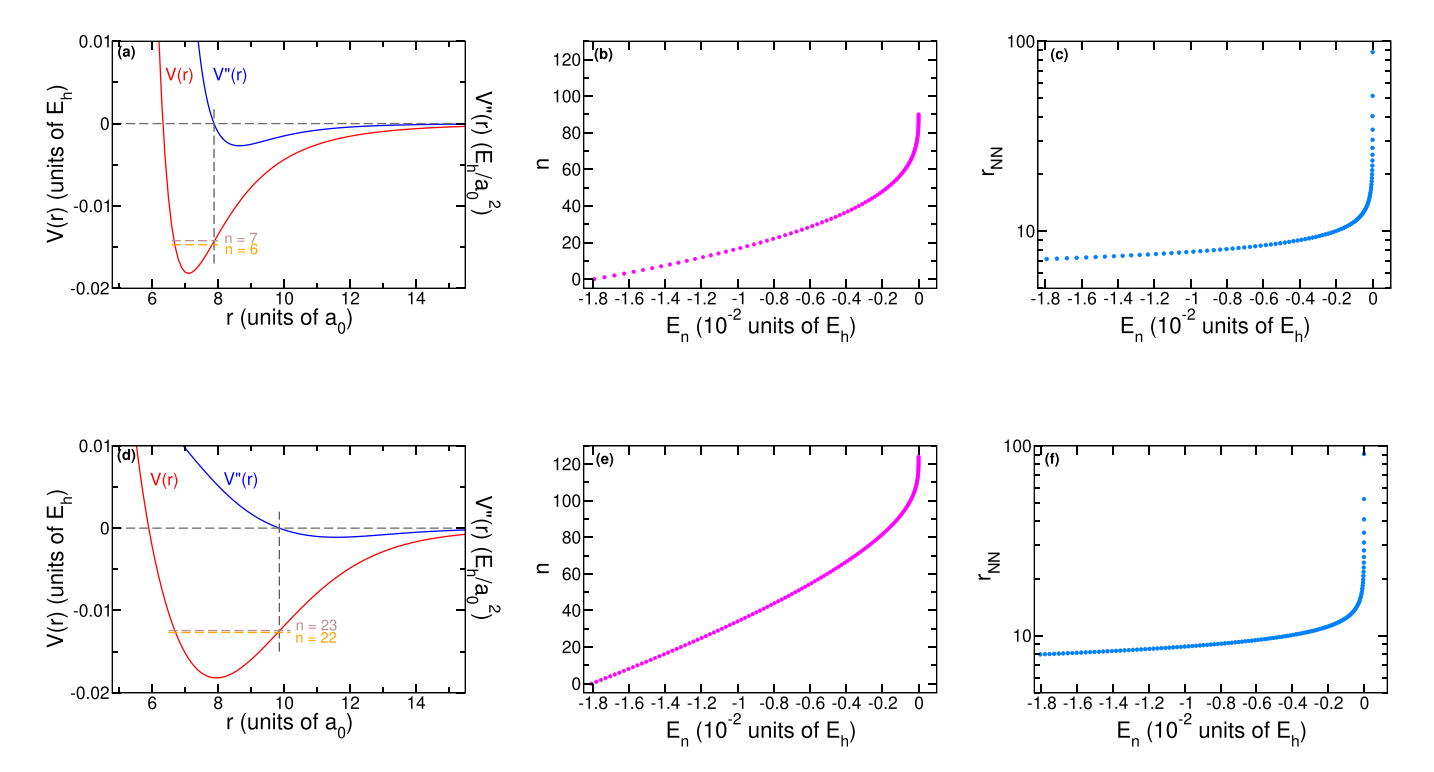


FIG. 1. Potential (also the second-order derivatives) as a function of (a) interatomic separation, (b) eigenstate spectra, and (c) matrix elements of operator \hat{r} sorted by eigenvalues for the Lennard-Jones potential. (d)–(f) Same results for the $X^1\Sigma_g^+$ potential of two interacting rubidium atoms [29].

where

$$b_{nl}(t) = -i\langle n|[\hat{r}(t), \hat{p}(0)]|l\rangle$$

= $-i\sum_{k} (e^{iE_{nk}t} r_{nk} p_{kl} - e^{iE_{kl}t} p_{nk} r_{kl}),$ (11)

with $E_{nl} \equiv E_n - E_l$, $r_{nl} \equiv \langle n|\hat{r}(0)|l\rangle$, and $p_{nl} \equiv \langle n|\hat{p}(0)|l\rangle$. Since $[\hat{H}, \hat{r}(0)] = -i\hat{p}(0)/\mu$, the matrix elements of the momentum operator can be written as $p_{nl} = i\mu E_{nl}r_{nl}$. Substituting this relation into Eq. (11), we have

$$b_{nl}(t) = \mu \sum_{k} r_{nk} r_{kl} (E_{kl} e^{iE_{nk}t} - E_{nk} e^{iE_{kl}t}).$$
 (12)

This method provides a concise framework for calculating the OTOC [17].

The eigenstate energy levels and wave functions are numerically solved by diagonalizing the exact Hamiltonian of the nuclear motion with an equidistant grid in the discrete-variable representation (DVR) method [30], where we choose the interatomic distance from $3a_0$ to $1500a_0$ with a step size of $0.01a_0$. Note that computing the OTOC for eigenstate $|n\rangle$ requires a sum over eigenstates $|l\rangle$ and $|k\rangle$ distinct from $|n\rangle$. For $|n\rangle$ too high in energy, this sum may require states above the dissociation threshold, which are not computed by the DVR method. For this reason, in what follows we restrict n to somewhat below the last bound state of the potentials, where we can ensure convergence of $C_n(t)$ to approximately 1%.

IV. RESULTS

A. Potential and eigenvalue spectrum

The two potentials are shown in Figs. 1(a) and 1(d) (red lines). Also depicted are the energy spectrum [Figs. 1(b) and 1(e)] and the mean interatomic separation $r_{\rm NN}$ [Figs. 1(c) and 1(f)] of these potentials. We can see that even with the same well depth, the Lennard-Jones potential supports fewer bound states than the realistic $X^1\Sigma_g^+$ potential due to its narrower potential shape.

A key component in describing the OTOC in a one-dimensional potential, as described above, is the curvature of the potential: Regions of coordinates where this curvature is negative are expected to correlate roughly to exponential OTOC growth. For this reason, the second derivative of the potentials is also shown (blue) in Figs. 1(a) and 1(d). Also shown is the range of n where the potential at the classical outer turning point nearly coincides with the transition from positive to negative curvature. As shown, this point is between n = 6 and 7 for the Lennard-Jones potential and between n = 22 and 23 for the realistic rubidium dimer potential. This is therefore the scale of n on which the transition to an exponentially growing OTOC may be expected to set in.

B. OTOC calculation

Beginning with the low-energy part of the spectrum, Fig. 2(a) shows the time evolution of the OTOC for selected energy eigenstates $|n\rangle$ of the Lennard-Jones potential. For the vibrational ground state n=0 and first-excited (n=1) states, the OTOC merely oscillates in time, consistent with the bottom of this potential being approximately harmonic.

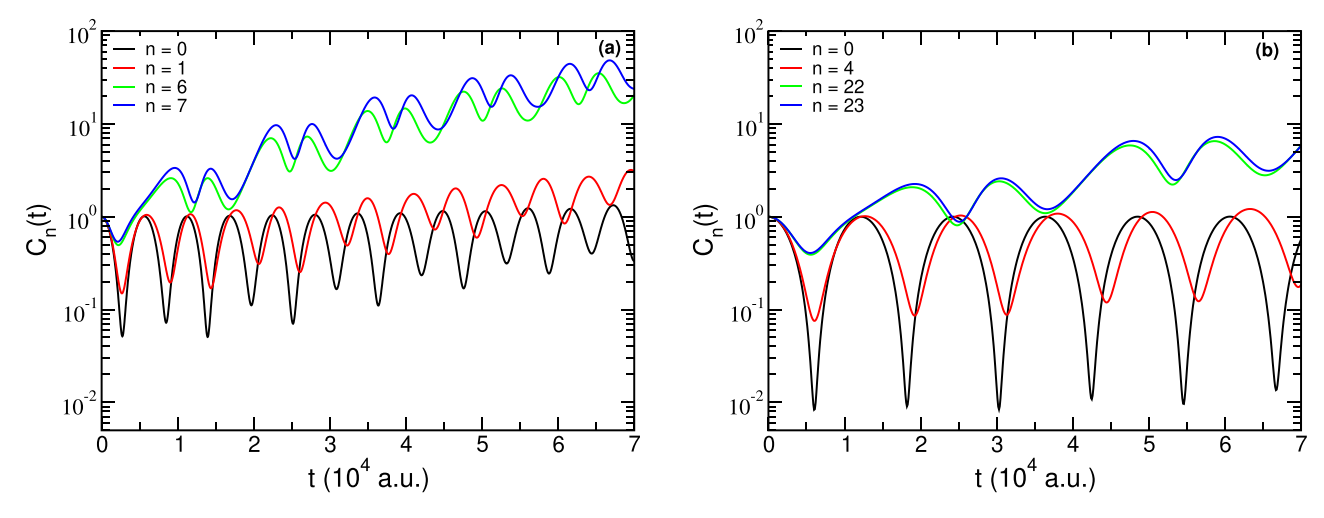


FIG. 2. OTOCs of lower-energy modes for (a) the Lennard-Jones potential and (b) the Rb₂ $X^1\Sigma_g^+$ potential.

The period of oscillation is about 5520 a.u., consistent with the equivalent harmonic oscillator. Slightly higher in the spectrum, for n = 6, 7, the OTOC experiences a brief burst of exponential-like growth up to approximately 10^{-4} a.u., before again varying quasisinusoidally. Recall that this is the approximate value of n at which exponential growth may be expected to start, but it has not yet taken over decisively.

Similarly, for the realistic rubidium $X^1\Sigma_g^+$ potential as shown in Fig. 2(b), the OTOC for the low-lying states n=0,4 varies sinusoidally. Higher in the spectrum, at n=22,23, the brief exponential behavior occurs. This behavior is again suggestive of the transition to exponential growth of the OTOC, as expected.

We compute the OTOCs as a function of t for each energy level n in the high-energy modes, which better exhibit exponential growth, at least for a short time. This behavior is shown for several values of n in Fig. 3. For the states shown, there is a clear region where the OTOC grows exponentially, and the time interval over which the exponential growth occurs is different for each eigenstate n. For each potential, a

representative exponential fit is shown as a green dashed line, fitting the OTOC for the n=20 level of the Lennard-Jones potential and the n=70 level of the rubidium dimer potential.

Fitting each such curve to the form $\alpha \exp(\lambda_{OTOC} t)$ defines an n-dependent sensitivity parameter λ_{OTOC} . We refer to this quantity as a sensitivity parameter, rather than a Lyapunov exponent, recognizing that these one-dimensional systems are integrable. The sensitivity parameters extracted from this kind of exponential fit, for a number of different eigenstates n, are shown as the red circles in Figs. 4(a) and 4(c), for the two potentials. The error bars represent a 95% confidence interval for the fits. The parameter λ_{OTOC} shows a definite trend, first rising and then falling, as a function of n in this part of the spectrum. The cyan squares and green triangles represent simple approximations, given in the next section.

An essential feature in any exponential growth trend is that the growth occurs for a sufficient time to identify it as exponential. In the present case, each OTOC grows exponentially over some time interval Δt , over which time the fit is

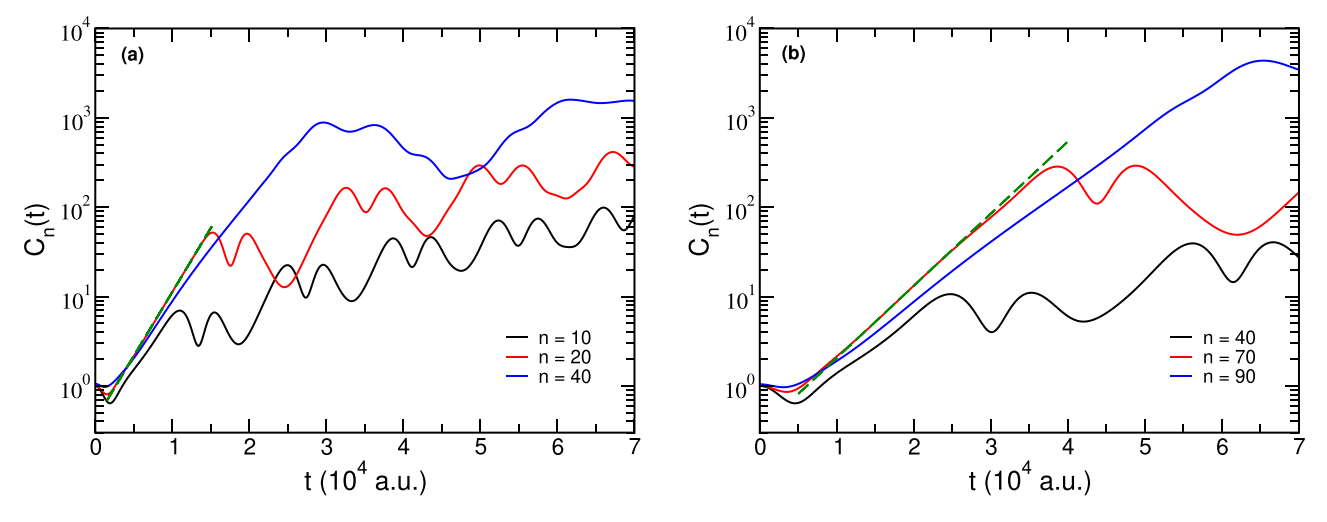


FIG. 3. OTOCs of high-energy modes for (a) the Lennard-Jones potential and (b) the Rb₂ $X^1\Sigma_g^+$ potential. The green dashed line is fitted with the exponential expression, as discussed in the text.

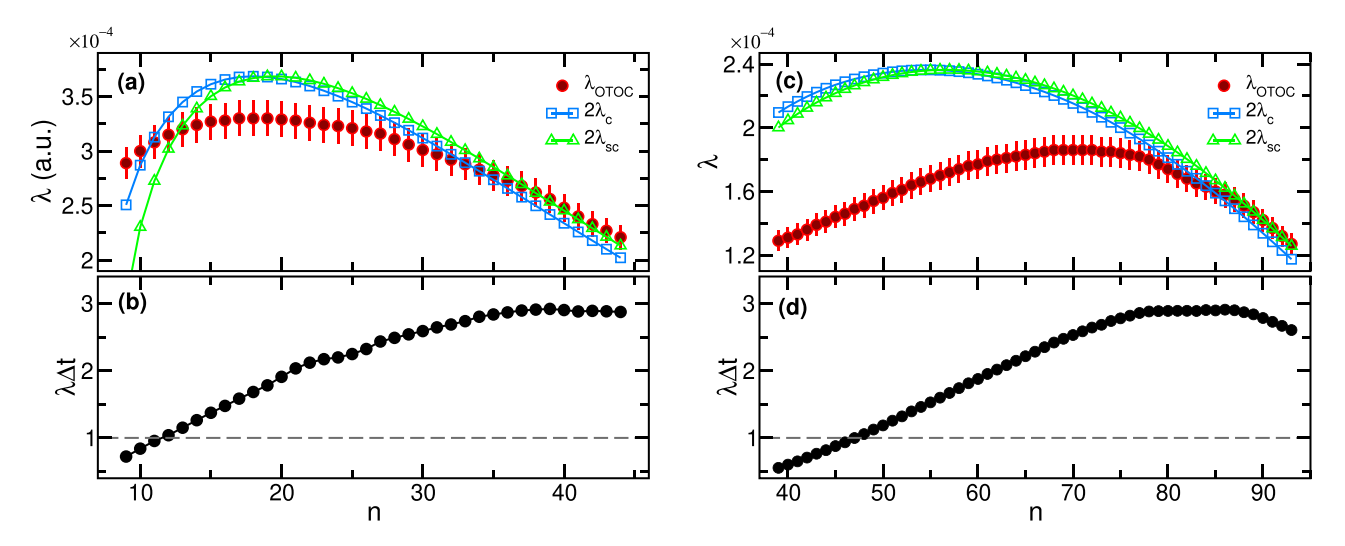


FIG. 4. Plots for (a) the Lennard-Jones potential and (b) the Rb₂ $X^1\Sigma_g^+$ potential. (a) and (c) The *n* dependence of the quantum sensitivity parameters λ_{OTOC} . The red closed circles are the fit values, the cyan open squares are the antiharmonic approximation at the outer classical turning points, and the green open triangles are the antiharmonic approximation at the wave-function maxima. (b) and (d) Confidence of the fit process, with Δt the fitting time interval.

constructed. If this time is short compared to the derived exponential time constant, then it is difficult to say the behavior is truly exponential. Therefore, we track the product $\lambda_{\text{OTOC}} \Delta t$ versus n in Figs. 4(b) and 4(d). If this product is greater than unity, then the exponential growth endures for at least one time constant. Over most of the spectrum shown, the product is indeed larger than one, meaning that the exponential growth is meaningful. This condition breaks down near the transition region, n=6, 7 for the Lennard-Jones potential and n=22, 23 for the rubidium dimer $X^1\Sigma_g^+$ potential, where the transition to exponential growth is incomplete.

V. INTERPRETATION

As we can see in Fig. 2, the OTOC is reasonably oscillatory for low-energy levels of the potentials we have considered, which are approximately harmonic. It is only higher in the spectrum in which $C_n(t)$ can grow exponentially, as shown in Fig. 3. Concomitant with this, the higher-energy levels have wave functions with large amplitude at the outer classical turning point r_c . Since the OTOC is an average over the wave function, it therefore arises rather locally from points near r_c . This is not unreasonable, as the sensitive dependence on the initial condition can surely depend on what that initial condition actually is.

A. Classical sensitivity

In any event, this localization in r allows a closer comparison to be made between the classical and quantum-mechanical versions. For example, the classical motion may as well be something that starts at $r = r_0$, close to r_c , and remains close to that point. In the neighborhood of r_c , we expand the potential to quadratic order,

$$V(r) \approx V(r_c) + V'(r_c)(r - r_c) + \frac{1}{2}V''(r_c)(r - r_c)^2$$

= $\frac{1}{2}V''(r_c)(r - r_d)^2$, (13)

where in the second line we ignore an overall constant and define $r_d = r_c - V'(r_c)/V''(r_c)$. For the initial condition r_0 in the vicinity of r_c , the solution to the equation of motion $m\ddot{r} = -\partial V(r)/\partial r$ is

$$r(t) = r_d + (r_0 - r_d) \cos\left(\sqrt{\frac{V''(r_c)}{\mu}}t\right) + \frac{p_0}{\sqrt{\mu V''(r_c)}} \sin\left(\sqrt{\frac{V''(r_c)}{\mu}}t\right)$$
(14)

if $V''(r_c) > 0$ and

$$r(t) = r_d + (r_0 - r_d) \cosh\left(\sqrt{\frac{-V''(r_c)}{\mu}}t\right) + \frac{p_0}{\sqrt{-\mu V''(r_c)}} \sinh\left(\sqrt{\frac{-V''(r_c)}{\mu}}t\right)$$
(15)

if $V''(r_c) < 0$. From these expressions it is clear that classical sensitivity to the initial condition occurs, approximately, only when the potential has local negative curvature, leading to divergence $e^{\lambda_c t}$, in terms of a classical sensitivity parameter

$$\lambda_c = \sqrt{\frac{|V''(r_c)|}{\mu}}. (16)$$

B. Quantum sensitivity

A completely analogous situation holds in the quantummechanical case. Assuming a quadratic potential in the quantum Hamiltonian

$$\hat{H} = \frac{\hat{p}^2}{2\mu} + \frac{1}{2}V''(r_c)(\hat{r} - r_d)^2, \tag{17}$$

(23)

the Heisenberg position operator is evaluated using the Baker-Campbell-Hausdorff lemma, similar to what one does for the standard harmonic oscillator [31]. For our present purposes, we consider only the case of negative curvature of the potential, where the operator becomes

$$\hat{r}(t) = r_d + \left[\hat{r}(0) - r_d\right] \cosh\left(\sqrt{\frac{-V''(r_c)}{\mu}}t\right) + \frac{\hat{p}(0)}{\sqrt{-\mu V''(r_c)}} \sinh\left(\sqrt{\frac{-V''(r_c)}{\mu}}t\right).$$
(18)

Thus

$$[\hat{r}(t), \hat{p}(0)] = i \cosh\left(\sqrt{\frac{-V''(r_c)}{\mu}}t\right). \tag{19}$$

Because the OTOC is defined in terms of the square of this quantity, its exponential growth in this approximation would be proportional to $\{\exp[\sqrt{V''(r_c)/\mu t}]\}^2 = e^{2\lambda_c t}$, that is, at a rate twice that of the classical exponential growth. The growth rate $2\lambda_c$ is plotted in Fig. 4.

A slightly better estimate of the OTOC's growth rate would evaluate the commutator, not at the classical turning point r_c but at a nearby point r_m where the wave function is maximal. To this end, we make a linear approximation of the potential near the turning point,

$$V(r) \approx E + V'(r_c)(r - r_c). \tag{20}$$

Defining the characteristic length scale $\bar{r} = (\frac{1}{2\mu V'(r_c)})^{1/3}$ and in terms of the dimensionless variable $z = (r - r_c)/\bar{r}$, the resulting Schrödinger equation becomes

$$\frac{d^2\psi}{dz^2} - z\psi = 0. \tag{21}$$

The solution to this is the usual Airy function, which, to a good approximation, is maximal at z = -1, whereby our bound-state wave functions are maximal at $r = r_m$, where

$$r_m = r_c - \bar{r} = r_c - \left(\frac{1}{2\mu V'(r_c)}\right)^{1/3}.$$
 (22)

This quantity of course takes a different value for each bound state n. The results of this approximation are also plotted in Fig. 4. The agreement with the quantum OTOC is slightly improved, especially at high n.

Using this result, we define a corrected semiclassical version

of the OTOC growth rate $2\lambda_{sc}$, where

VI. CONCLUSIONS AND OUTLOOK

We have verified, in realistic molecular potentials, a trend that has been seen elsewhere, namely, that exponential growth of the classical sensitivity and the quantum-mechanical OTOC are linked, even in the absence of chaotic behavior. In the molecular system we have considered, the characteristic longrange van der Waals tail of these potentials produces a fairly explicit transition between regular and sensitive behavior of the dynamics as a function of the energy level. Molecules are thus revealed as objects of variable sensitivity by this measure.

The lessons learned from this work should inform the investigation of far more complex molecules, in particular the ultracold lanthanide dimers alluded to at the outset. Such molecules are expected to be truly chaotic, rather than merely sensitive, as the models presented here were. Thus, for example, Dy₂ molecules just below their dissociation threshold should exhibit exponential growth of their OTOCs in some way distinct from the sensitivity we have described, which may lead to additional insight into their dynamics. This dynamics has the advantage that the OTOC will depend not only on the level considered, but also on the magnetic field applied in the laboratory, which is suspected to increase the degree of chaos in the molecules [25].

Looking ahead, we note that the exponential growth of the OTOC at relatively short times is not the only characteristic designating chaotic behavior. Indeed, quantum chaotic systems have been identified for which the quantum-mechanical OTOC does not appear to grow exponentially [32,33]. Nevertheless, the long-time behavior was shown to oscillate in non-chaotic systems, but to saturate in chaotic systems [2,33–35]. Though we have not emphasized this, in the present integrable Lennard-Jones and rubidium dimer examples, the OTOC indeed oscillates at long times. It is expected that, instead, saturation will occur for the case of Dy₂.

ACKNOWLEDGMENT

This paper is based upon work supported by the National Science Foundation under Grants No. PHY 1734006 and No. PHY 2110327.

only the case of negative curvature of the potenhe operator becomes $\lambda_{\rm sc} = \sqrt{\frac{|V''(r_m)|}{\mu}}.$ This quantity of course takes a different value for

^[1] E. B. Rozenbaum, S. Ganeshan, and V. Galitski, Phys. Rev. Lett. 118, 086801 (2017).

^[2] I. García-Mata, M. Saraceno, R. A. Jalabert, A. J. Roncaglia, and D. A. Wisniacki, Phys. Rev. Lett. **121**, 210601 (2018).

^[3] H. Gharibyan, M. Hanada, B. Swingle, and M. Tezuka, J. High Energy Phys. 04 (2019) 082.

^[4] J. Chávez-Carlos, B. López-del Carpio, M. A. Bastarrachea-Magnani, P. Stránský, S. Lerma-Hernández, L. F. Santos, and J. G. Hirsch, Phys. Rev. Lett. 122, 024101 (2019).

^[5] R. J. Lewis-Swan, A. Safavi-Naini, J. J. Bollinger, and A. M. Rey, Nat. Commun. 10, 1581 (2019).

- [6] E. M. Fortes, I. García-Mata, R. A. Jalabert, and D. A. Wisniacki, Phys. Rev. E 100, 042201 (2019).
- [7] T. Ali, A. Bhattacharyya, S. S. Haque, E. H. Kim, N. Moynihan, and J. Murugan, Phys. Rev. D 101, 026021 (2020).
- [8] M. Rautenberg and M. Gärttner, Phys. Rev. A 101, 053604 (2020).
- [9] K. Y. Bhagat, B. Bose, S. Choudhury, S. Chowdhury, R. N. Das, S. G. Dastider, N. Gupta, A. Maji, G. D. Pasquino, and S. Paul, Symmetry 13, 44 (2020).
- [10] T. Xu, T. Scaffidi, and X. Cao, Phys. Rev. Lett. 124, 140602 (2020).
- [11] S. Pilatowsky-Cameo, J. Chávez-Carlos, M. A. Bastarrachea-Magnani, P. Stránský, S. Lerma-Hernández, L. F. Santos, and J. G. Hirsch, Phys. Rev. E 101, 010202(R) (2020).
- [12] J. Wang, G. Benenti, G. Casati, and W.-G. Wang, Phys. Rev. E 103, L030201 (2021).
- [13] C. Yin and A. Lucas, Phys. Rev. A 103, 042414 (2021).
- [14] A. Bhattacharyya, W. Chemissany, S. S. Haque, and B. Yan, Eur. Phys. J. C 82, 1 (2022).
- [15] C. Zhang, P. G. Wolynes, and M. Gruebele, Phys. Rev. A 105, 033322 (2022).
- [16] A. I. Larkin and Y. N. Ovchinnikov, Sov. Phys. JETP 28, 1200 (1969).
- [17] K. Hashimoto, K. Murata, and R. Yoshii, J. High Energy Phys. 10 (2017) 138.
- [18] T. Akutagawa, K. Hashimoto, T. Sasaki, and R. Watanabe, J. High Energy Phys. 08 (2020) 013.
- [19] K. Hashimoto, K.-B. Huh, K.-Y. Kim, and R. Watanabe, J. High Energy Phys. 11 (2020) 068.
- [20] L.-C. Qu, J. Chen, and Y.-X. Liu, Phys. Rev. D 105, 126015 (2022).
- [21] T. Morita, Phys. Rev. D 106, 106001 (2022).

- [22] P. Romatschke, J. High Energy Phys. 01 (2021) 030.
- [23] A. Frisch, M. Mark, K. Aikawa, F. Ferlaino, J. L. Bohn, C. Makrides, A. Petrov, and S. Kotochigova, Nature (London) 507, 475 (2014).
- [24] T. Maier, H. Kadau, M. Schmitt, M. Wenzel, I. Ferrier-Barbut, T. Pfau, A. Frisch, S. Baier, K. Aikawa, L. Chomaz, M. J. Mark, F. Ferlaino, C. Makrides, E. Tiesinga, A. Petrov, and S. Kotochigova, Phys. Rev. X 5, 041029 (2015).
- [25] C. Makrides, M. Li, E. Tiesinga, and S. Kotochigova, Sci. Adv. 4, eaap8308 (2018).
- [26] J. McCann, J. L. Bohn, and L. D. Augustovičová, Phys. Rev. A 103, 042812 (2021).
- [27] J. L. Bohn, *A Student's Guide to Analytical Mechanics* (Cambridge University Press, Cambridge, 2018).
- [28] M. G. Calkin, Lagrangian and Hamiltonian Mechanics (World Scientific, Singapore, 1996).
- [29] C. Strauss, T. Takekoshi, F. Lang, K. Winkler, R. Grimm, J. Hecker Denschlag, and E. Tiemann, Phys. Rev. A 82, 052514 (2010).
- [30] E. Tiesinga, C. J. Williams, and P. S. Julienne, Phys. Rev. A 57, 4257 (1998).
- [31] J. J. Sakurai and E. D. Commins, Modern Quantum Mechanics (American Association of Physics Teachers, College Park, 1995).
- [32] B. Bertini, P. Kos, and T. Prosen, Phys. Rev. Lett. 121, 264101 (2018).
- [33] D. Marković and M. Čubrović, J. High Energy Phys. 05 (2022) 023.
- [34] P. D. Bergamasco, G. G. Carlo, and A. M. F. Rivas, Phys. Rev. Res. 1, 033044 (2019).
- [35] R. A. Kidd, A. Safavi-Naini, and J. F. Corney, Phys. Rev. A 103, 033304 (2021).